MRS Communications (2016), 6, 226–233

doi:10.1557/mrc.2016.34

MRS Communications

Functional Oxides Research Letter

Titanium dioxide nanowires modified tin oxide hollow spheres for dye-sensitized solar cells

Yajie Wang, Chengbin Fei, Rong Zhang, and **Lixue Guo,** Beijing Institute of Nanoenergy and Nanosystems, Chinese Academy of Sciences , Beijing 100083, China; National Center for Nanoscience and Technology (NCNST), Beijing 100083, China
Ting Shen, and **Jianjun Tian,** Advanced Material and Technology Institute, University of Science and Technology, Beijing 100083, China
Guozhong Cao, Beijing Institute of Nanoenergy and Nanosystems, Chinese Academy of Sciences , Beijing 100083, China; National Center for Nanoscience and Technology (NCNST), Beijing 100083, China; Department of Materials and Engineering, University of Washington, Seattle, WA 98195-2120, USA

Address all correspondence to Guozhong Cao at **gzcao@u.washington.edu** and Jianjun Tian at **tianjianjun@mater.ustb.edu.cn**

(Received 24 June 2016; accepted 22 August 2016)

Abstract

Tin oxide (SnO_2) hollow spheres modified with titanium dioxide (TiO_2) nanowires (NWs) synthesized by sequential hydrothermal reactions were investigated as photoanodes for dye-sensitized solar cells. Not only does the hydrothermal treatment form numerous short TiO_2 NWs on the surface of SnO_2 spheres, but also passivates the surface of SnO_2. Consequently, the specific surface area of the photoanode and dye loading are almost doubled, at the same time the surface defects and charge recombination are both appreciably reduced. As a result, the short-circuit photocurrent density and open-circuit photovoltage both greatly increased. The power conversion efficiency of the solar cells increases from 0.4% to 2.9%.

Introduction

Since titanium dioxide (TiO_2) nanoparticles first has been combined with dye molecules to fabricate low-cost photovoltaic device in 1991, dye-sensitized solar cells (DSCs) have attracted extensive interest in the past few decades as a promising candidate to convert solar energy to electricity.[1–3] Although using TiO_2 nanoparticle films with collaborated silyl-anchor and carboxy-anchor dyes has achieved a power conversion efficiency of higher than 14% in 2015,[4] TiO_2 as photoanodes in DSCs still face many challenges.[5,6] It has become a focus recently that looking for alternative metal oxide semiconductors with wide band gap and good photoelectrochemical properties.[7–10] ZnO nanostructures for DSC applications has shown that they can offer large specific surface areas with well-controlled morphologies, direct electron pathways with much higher electron mobility, and also can reduce the combination rate when the surface defects are properly controlled.[11–13] Tin oxide (SnO_2) as a promising alternative semiconductor has many advantages for DSCs: (1) good electron mobility, indicating electron transport fast in photoanodes and (2) large band gap (3.6 eV) and more-negative conduction band minimum, which can enhance the light harvesting in the near-infrared spectral region when combined with small band gap sensitizer.[14]

Many different nanostructures of SnO_2 have been synthesized with a variety of methods with emphasis to avoid its weakness, such as electron recombination and surface defects.[15] Low-dimensional nanostructures of SnO_2 have been widely reported, including zero-dimensional (0D) nanoparticles,[16] one-dimensional (1D) nanorods,[17] nanobelts,[18] nanotube,[19] and nanowires (NWs).[20] The process of SnO_2 nanostructure synthesis is always related to chemical reaction of tin precursor and crystallization of SnO_2. Different reaction parameters, such as the concentration of precursor solution, pH value and addition agent, will influence the morphology of SnO_2 nanostructure eventually. In addition, in order to solve the problem that less dye adsorption of SnO_2 owing to lower isoelectric point (i.e.p., at pH 4–5), coating other metal oxide such as TiO_2 (i.e.p., at pH 6–7)[21] can increase the cell efficiency of DSCs.[22,23] For example, in 2011 Wu et al.[24] synthesized hierarchical structure consisting of 2D SnO_2 nanosheets and other metal oxides to increase the open-circuit photovoltage. Among the large number of materials, 1D TiO_2 NWs with superior light-scatting ability can provide a direct way to transport electrons and enhance the performance of the whole solar cells.[25–29] In addition, TiO_2 NWs can also provide a rapid electron transfer and reduce the electron recombination rate. As a result, the power conversion efficiency is greatly improved.[30]

In this paper, SnO_2 hollow spheres (HSs) made of SnO_2 nanoparticles modified with TiO_2 NWs were employed as photoanodes for DSCs. The uniform SnO_2 spheres are synthesized without using any template through a hydrothermal method, which makes the reaction product with better crystallinity and less surface defects. When such SnO_2 HSs were modified with TiO_2 NWs, the large specific surface area, less surface defect, and good light-scatting properties make it an attractive

alternative photoanode materials with high dye loading, effective light absorption, direct electron transport path, and reduced charge recombination. The short-circuit photocurrent density and open-circuit photovoltage both have been greatly increased. The power conversion efficiency of the solar cell based on SnO_2 HSs coated with 3D TiO_2 NWs as photoanodes reached 2.9%, which presents six times of enhancement as compared with the DSCs with SnO_2 HS anodes.

Experimental methods

Synthesis of SnO_2 HSs

The 10 mmol of $SnCl_2$ (1 M in concentration) were dissolved in 10 mL mixture of ethanol and hydrochloric acid (9:1 in volume) and stirred for 5 min. The solution was transferred to a 35 mL reaction tube and reactor cavity of the CEM Discover microwave system. The synthesis parameters were set as: T = 180 °C, dwell time = 2 h, power = 120 w, and pressure = 17 bars. After cooling naturally, the precipitate was harvested by centrifugation at 8000 rpm for 30 min and washed thoroughly with deionized (DI) water for at least three times. The brown powder was calcined at 450 °C for 3 h to remove the inner carbon sphere completely to obtain SnO_2 HSs.

Preparation of SnO_2 paste

SnO_2 powders (0.18 g) were placed in an agate mortar, and 5.0 mL of ethanol was added dropwise into the mortar. The SnO_2 powders were ground for 30 min. The ground SnO_2 was then transferred to a solution of terpineol (0.73 g) and ethyl cellulose (0.09 g) in a 10 mL beaker under magnetic stirring. The dispersion was homogenized by means of ultrasonic and magnetic stirring overnight. A layer of SnO_2 film was prepared by the doctor blade technique. The film was sintered at 500 °C for 60 min in air to remove any organic compounds.

Synthesis of SnO_2 HSs coated with TiO_2 NWs

$K_2TiO(C_2O_4)_2$ (0.35 g) was added to the mixture solvent containing diethylene glycol (DEG) and DI water in different volume ratios (0:20, 1:19, 10:10, 19:1), while the total volume of the solution was 20 mL. The solution was transferred to a 50 mL Teflon-lined stainless steel autoclave. Then as-prepared SnO_2 films were placed at an angle against the wall of the Teflon-liner with the film side facing down. The hydrothermal synthesis was carried out by putting the autoclave in an oven at 180 °C for 6 h with a heating rate of 5 °C/min and air-cooled to room temperature naturally. Subsequently, the samples were rinsed with DI water, ethanol, and sintered at 500 °C for 60 min in air to increase crystallinity.

Fabrication of DSCs

The electrodes with a cell area of 0.25 cm^2 were immersed in a 0.25 mM N719 sensitizer dye for 18 h. The counter-electrodes were Pt-coated fluorine doped tin oxide (FTO), and the electrolyte was contained I^-/I^{3-} redox. The DSCs with TiO_2 NWs treatment (DEG: DI = 1:19) and without TiO_2 NWs treatment were designed by SnO_2 HS–TiO_2 NW and SnO_2 HS.

Characterization

X-ray diffraction (XRD) measurements were conducted on an X'Pert PROS (Philips Co.) with a radiation of Cu K_α (λ = 1.54060 Å). Hitachi SU8020 scanning electron microscope (SEM) system was employed to analyze the morphology. The absorption spectra were measured using a Shimadzu UV-3600 spectrophotometer. N_2 adsorption–desorption isotherms were recorded on ASAP2020 instrument (Micromeritics Co.), and the specific surface areas [Brunauer–Emmett–Teller (BER)] were calculated using the BET equation. Desorption isotherm was used to determine the pore-size distribution using the Barret–Joyner–Halender (BJH) method. The photovoltaic characteristics of the solar cells were evaluated using simulated AM 1.5 sunlight with an output power of 100 mW/cm^2. The incident monochromatic photon-to-electron conversion efficiency (IPCE) plotted as a function of excitation wavelength were recorded IM6ex (Zahner, Germany) using light-emitting diodes (LED; λ = 455 nm) driven by Expot (Zahner, Germany). The electrochemical impedance spectroscopy (EIS) data were fit to the equivalent circuits by using Zview software (Scribner Associates). Impedance measurements were carried out under illumination from LED.

Results and discussion

Scheme 1 is the proposed schematic illustrating the formation process of the SnO_2 HSs and subsequent modification with

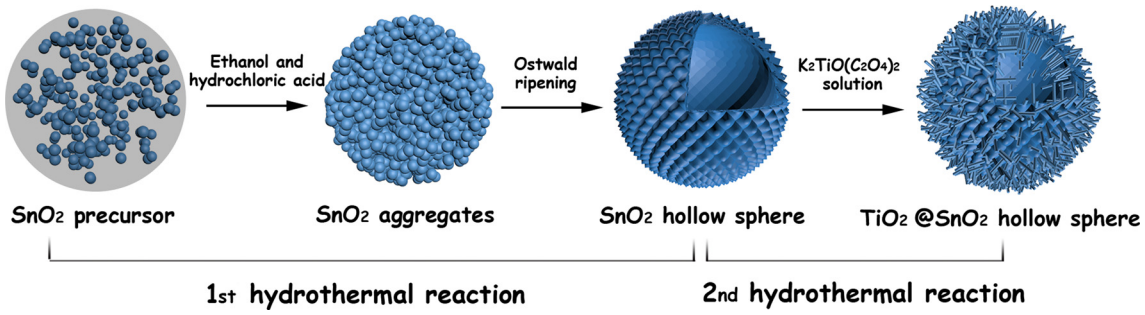

Scheme 1. The schematic of the formation processes for the SnO_2 HSs and the subsequent growth of TiO_2 NWs on the surface of SnO_2 HSs.

https://doi.org/10.1557/mrc.2016.34 Published online by Cambridge University Press

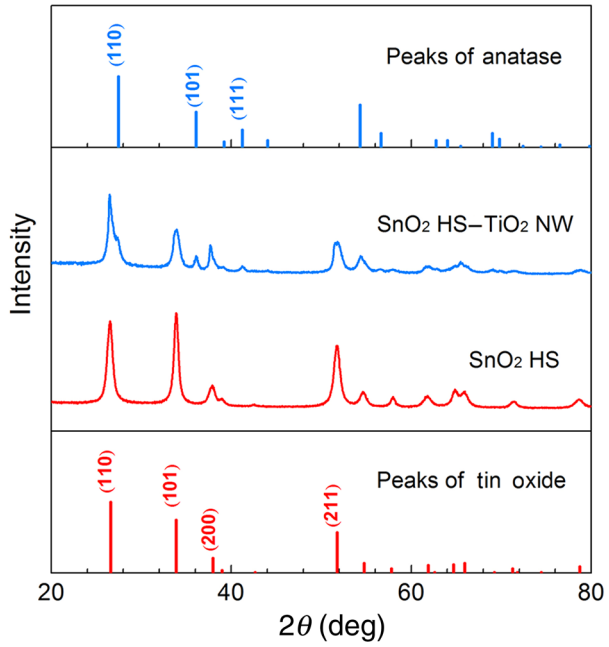

Figure 1. XRD patterns of SnO_2 HS and SnO_2 HS–TiO_2 NW powders showing SnO_2 HSs having a rutile crystal structure while TiO_2 NWs with an anatase crystal structure.

TiO_2 NWs. The formation of SnO_2 HSs without using templates could be ascribed to a simple Ostwald ripening process as reported in literature.[31] The solid spherical aggregates were first formed by the self-assembly of SnO_2 nuclei through the oxidation and hydrolysis reactions of Sn^{2+}. Since the particles that located in the inner cores have poor crystallinity as well as higher surface energies, they are more easily dissolved at high temperatures (fast kinetics in hydrothermal growth condition). With reaction proceeds, the interior cavities will be generated within the solid spheres, and hollow SnO_2 spheres can be obtained. Besides, the as-prepared thorn-like nanoparticles around the HSs probably can be explained by the acid etching effect of hydrochloric acid. The uniformly sized SnO_2 HSs of approximately 200 nm in diameter are composed of 15 nm nanoparticles, then blade coating on the FTO. The SnO_2 films are coated with TiO_2 NWs using the hydrothermal synthesis in the Teflon-liner stainless steel autoclave. In order to fabricate TiO_2 NWs, the SnO_2 films immersed in a solution with titanium potassium oxalate and a mixture solvent containing DEG and DI water. In reaction process, DEG plays a role as capping agent to control morphology of TiO_2 nanostructure by means of changing volume ratios of DEG and DI water.[32,33] The advantage of this hierarchical nanostructure lies in HSs provided with the large specific surface area and enhanced light scatting, at the same time TiO_2 NWs can provide a direct transport path for electrons transport. In addition,

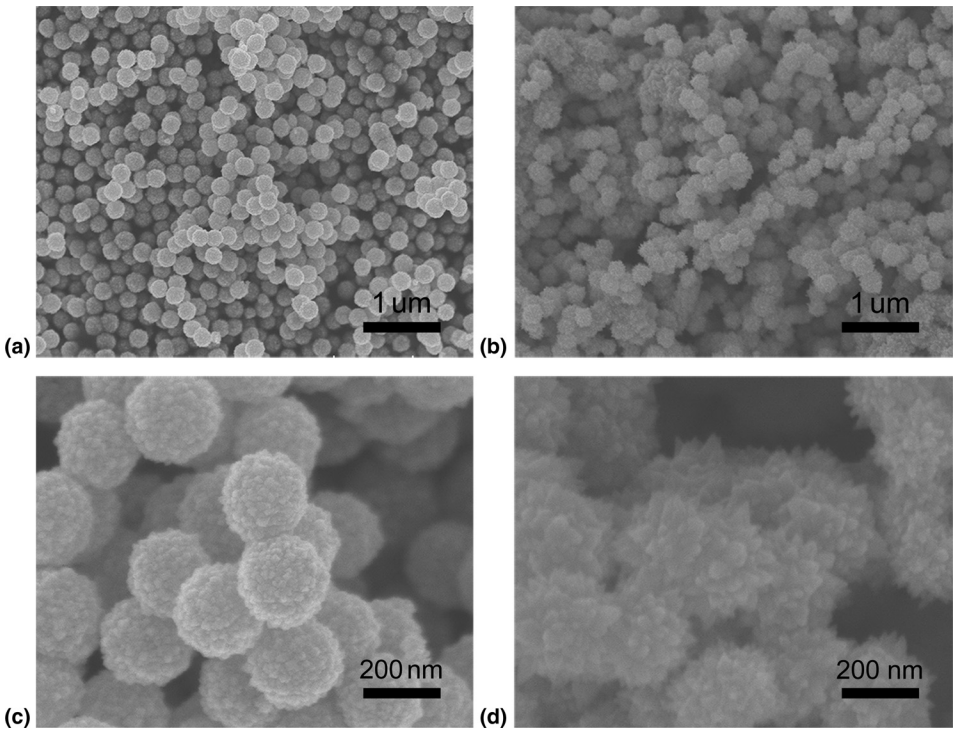

Figure 2. SEM images of: (a, c) SnO_2 HS nanostructure, (b, d) SnO_2 HS with TiO_2 NWs structure.

https://doi.org/10.1557/mrc.2016.34 Published online by Cambridge University Press

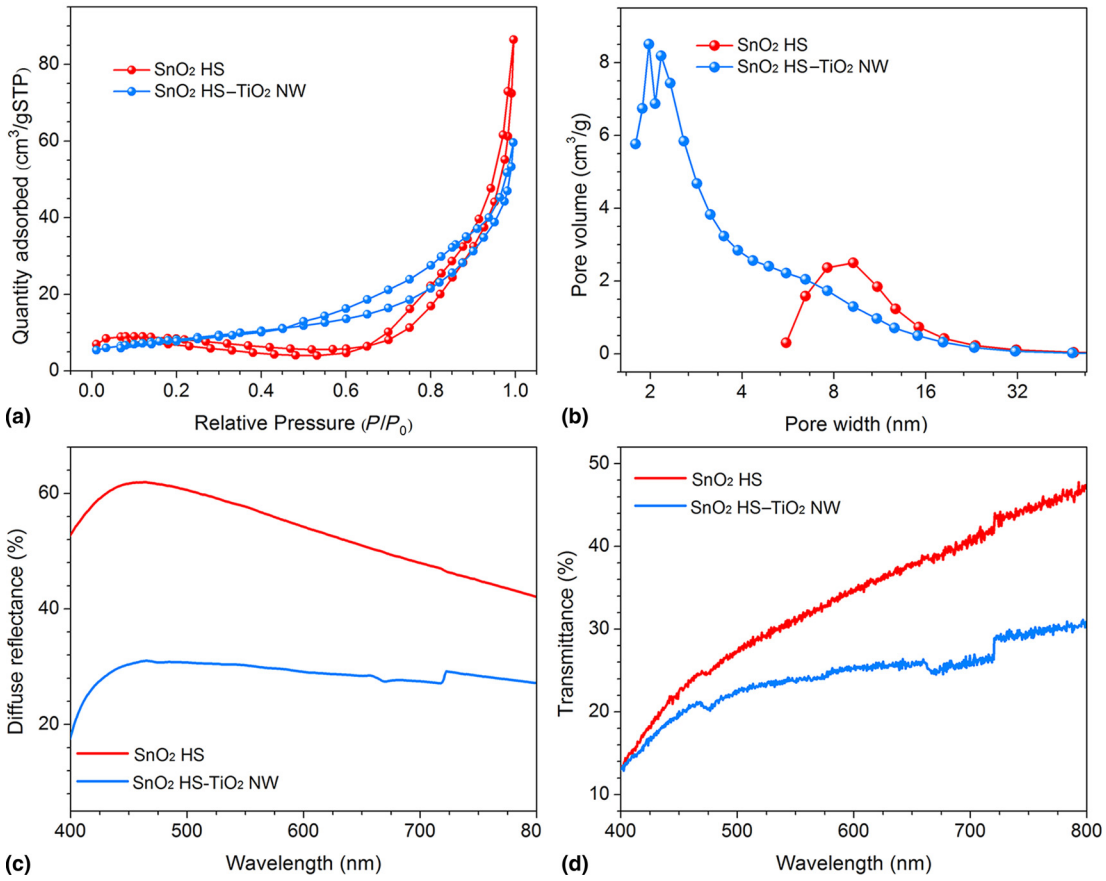

Figure 3. (a) Nitrogen adsorption and desorption isotherms at 77 K, and (b) the pore-size distribution of SnO_2 HS and SnO_2 HS–TiO_2 NW powders. (c) The diffuse reflectance curves and (d) transmission spectra of SnO_2 HS and SnO_2 HS–TiO_2 NW photoanodes without dye loading.

the surface of SnO_2 HS is also passivated by TiO_2 to reduce the surface defects.

To clearly show the composition changes in the materials, we measured the SnO_2 HSs, and SnO_2 HSs modified with TiO_2 samples with an x-ray diffractomer. As shown in Fig. 1, the XRD patterns of SnO_2 HS and SnO_2 HS–TiO_2 NW have undergone significant changes. SnO_2 HS powder has the tetragonal rutile structure with lattice constants of $a = 4.738$ and $c = 3.187$ Å, while SnO_2 HS–TiO_2 NW powder has the TiO_2 anatase structure with lattice constants of $a = 4.593$ and $c = 2.959$ Å. No other impurity crystal is detectable, which suggests that template-free growth can effectively form high-purity tetragonal rutile SnO_2 crystal and the subsequent hydrothermal growth results in the growth of anatase TiO_2 NWs.

Figures 2(a) and 2(c) are the different magnification SEM images of SnO_2 HSs. The template-free hydrothermal method can form SnO_2 HSs with almost identical appearance. A close look reveals that the SnO_2 HSs of 200 nm in diameter are the assembly of nanoparticles of 15 nm in diameter. Figures 2(b) and 2(d) show the different magnification SEM images of SnO_2 HS–TiO_2 NW structure. When titanium potassium oxalate exists in the mixture solvent containing DEG and DI water under sufficiently high temperature and long duration, it can form a globular structure consisting of TiO_2 NWs. It can also form TiO_2 NWs on the surface of SnO_2 HSs because of increasing active growth sites. Adjusting DEG and DI water volume ratios to 1:19, TiO_2 NWs grow with a diameter of 30–50 nm.

The SnO_2 HS and SnO_2 HS–TiO_2 NW powders were further characterized by means of nitrogen sorption isotherms at 77 K as shown in Fig. 3(a), and the corresponding pore-size distribution is presented in Fig. 3(b). It is found that the SnO_2 HSs have a very low BET surface area, only 20.8 m^2/g with an average BJH pore diameter of 17.3 nm and a pore volume of 0.15 cm^3/g. By contrast, the SnO_2 HS–TiO_2 NWs have 39.3 m^2/g BET surface area with BJH pore diameter 10.5 nm and 0.09 cm^3/g pore volume. Although it might look against the intuition, SnO_2 HS sample with relatively low pore volume and low BET surface area is reasonable. The nitrogen sorption isotherms through surface adsorption and capillary condensation are valid in the microporous and mesoporous regions. When the voids inside the SnO_2 HSs are larger than 100 nm, isotherms can have significant deviation. The isotherm for SnO_2 HSs in Fig. 3(a) demonstrated a substantial reduction in

https://doi.org/10.1557/mrc.2016.34 Published online by Cambridge University Press

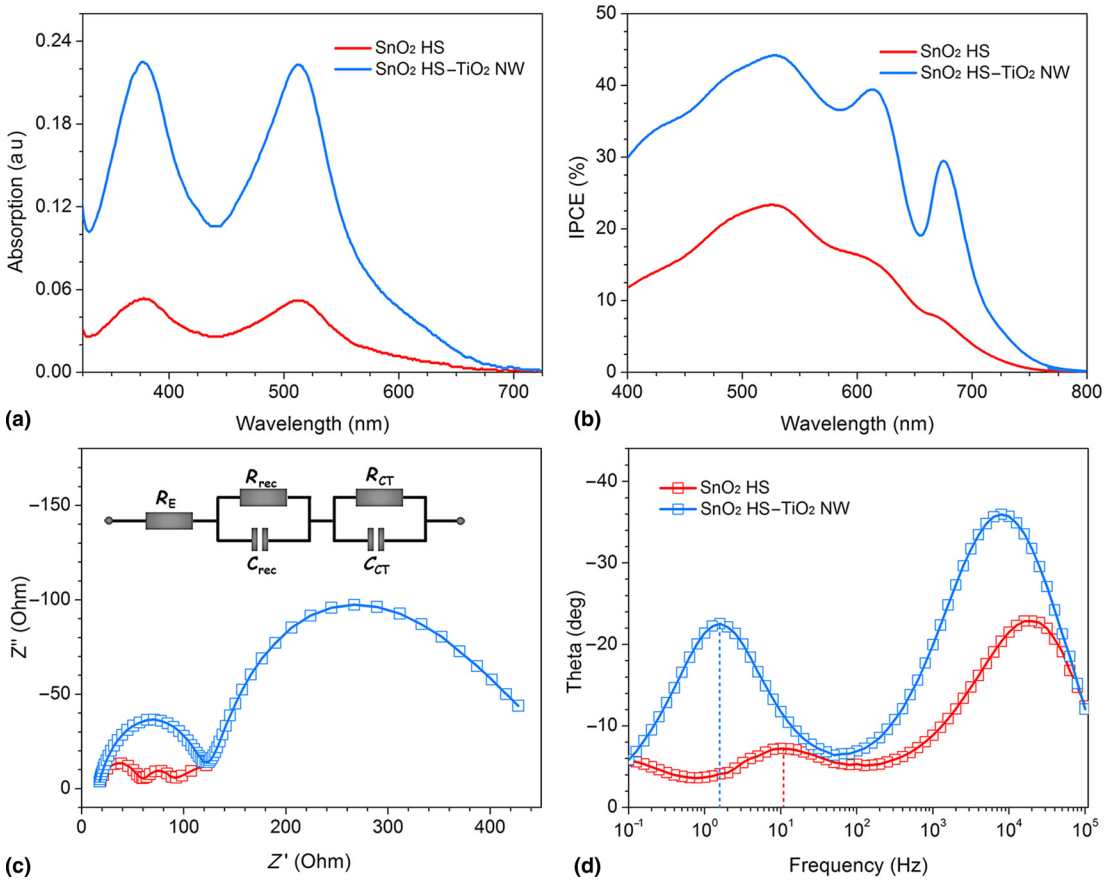

Figure 4. (a) The comparison of UV–vis absorption spectra of dyes dissolved in ethanol, unloaded from respective SnO_2 HS and SnO_2 HS–TiO_2 NW photoanodes; (b) IPCE spectra of DSCs with the two photoanodes; (c) the Nyquist plots; and (d) Bode curves of electrochemical impedance spectra of SnO_2 HS and SnO_2 HS–TiO_2 NW photoanodes with a forward bias of open-circuit voltage, the inset is an equivalent circuit of the solar cells.

adsorbed nitrogen volume at relative pressures ranging from 0.05 to 0.65, and suggested a possible capillary force-induced shrinkage and/or partial collapse of the porous structure. So the pore volume and possibly the BET surface area measured here with nitrogen sorption isotherms are most likely much smaller than the real values. TiO_2 NWs grown on the surface of SnO_2 HSs and filling the space between spheres would contribute to the increased BET surface area with reduced pore size and porosity. Figure 3(c) shows two films' light-scatting ability measured by the UV–vis diffuse reflectance spectroscopy, and reveals that the diffuse reflection of SnO_2 HS film is much higher than the SnO_2 HS–TiO_2 NW film. Here are three possible reasons about two films with different diffuse reflection: (1) the growth of TiO_2 NWs on the surface of SnO_2 HS layer would definitely increase the surface roughness, and thus reduce the light-scatting ability of the SnO_2 HS–TiO_2 NW film. (2) The SnO_2 HS–TiO_2 NW film would definitely have a lower packing density, which would contribute to a reduced diffuse reflection. (3) Although TiO_2 possesses the index of refraction of 2.488, appreciably higher than that of SnO_2, 2.006,[34] the amount of TiO_2 might be too small to make significant impact.

BET surface area differences between the sample SnO_2 HS and SnO_2 HS–TiO_2 NW also affect the amount of dye adsorption, and then have an impact on the performance of DSCs based on two different photoanodes. Figure 4(a) shows the curves of dye absorption and details summarized in Table I. Owing to the poor adsorption property of SnO_2 HS photoanode with dye molecules, it provides very low dye loading of 2.12×10^{-8} mol/cm^2. By contrast, TiO_2 have a good associativity with dye molecules and the loose structure because of the NWs existing and the value of dye loading in SnO_2 HS–TiO_2 NW photoanode is 7.64×10^{-8} mol/cm^2, more than three times of the amount of dye loaded on SnO_2 HS photoanode. The ameliorative dye loading can obviously improve the light harvesting, possibly resulting in the enhanced photocurrent density and subsequently the power conversion efficiency of the solar cells if other properties are kept the same. According to the BET surface area data, SnO_2 HS–TiO_2 NW sample has the specific surface area, 1.8 times larger than that of SnO_2 HS sample, whereas 3.6 times more dye loading than SnO_2 HS. The possible explanation for such differences in BET surface areas and in dye-loading data is ascribed to the different dye-loading ability of metal oxides stemming

https://doi.org/10.1557/mrc.2016.34 Published online by Cambridge University Press

Table I. Parameters of the BET testing results, impedance measurements and the amount of dye loaded in SnO_2 HS and SnO_2 HS–TiO_2 NW photoanodes.

DSCs	Surface area (m^2/g)	Pore volume (cm^3/g)	Dye loading ($\times 10^{-8}$ mol/cm^2)	τ_r (ms)	R_{rec} (Ω)	R_{ct} (Ω)
SnO_2 HS	21	0.15	2.12	15.9	33	43
SnO_2 HS–TiO_2 NW	39	0.09	7.64	100.5	203	107

from their different surface chemistry and surface energy, SnO_2 has less dye adsorption owing to its lower isoelectric point (i.e. p., at pH 4–5), while TiO_2 has higher isoelectric point (i.e.p., at pH 6–7).[21]

To further understand the photovoltaic properties of DSCs with the photoanode of SnO_2 HS and SnO_2 HS–TiO_2 NW, the IPCEs were characterized with the results shown in Fig. 4 (b). The IPCE is defined as the number of electrons detected in the external circuit produced by an incident photon at a given wavelength, related to electron injection efficiency, dye regeneration efficiency, charge collection efficiency, and light-harvesting efficiency.[35] The IPCE values of the solar cell constructed with SnO_2 HS–TiO_2 NW powder of about 45% are much higher than that of the device based on SnO_2 HS powder, of <25%. This figure clearly showed that the solar cells based on SnO_2 HS–TiO_2 NW electrode has better performances, attributing to better dye loading and light scattering in the whole wavelength region from 400 to 750 nm. It is noted that two photoanodes both have HS structures, which have a good impact on light-scattering properties in longer wavelength regions.[35]

The EIS measurements are carried out in the frequency range from 0.1 Hz to 100 kHz so as to study the interfacial charge transfer process in the DSCs based on SnO_2 HS and SnO_2 HS–TiO_2 NW photoanodes. As shown in Fig. 4(c), the Nyquist plots of the two photoanodes are measured at a forward bias of the open-circuit voltage under 100 mW/cm^2 and the equivalent circuit is presented as an inset. In general, the first semicircle occurring at high frequencies in the Nyquist plots presents the parallel connection of charge-transfer resistance (R_{ct}) and the interfacial capacitance (C_c) at the counter electrode/electrolyte interface, while the second semicircle at low-frequency region is the charge recombination resistance (R_{rec}) occurring at the metal oxide/dye/electrolyte interface and the chemical capacitance that stands for the change of electron density (C_{rec}). The charge transfer resistance of SnO_2 HS–TiO_2 NW is larger than that of SnO_2 HS, which probably means that the poor electron mobility of TiO_2 results in slower electron transfer process between the counter electrode and electrolyte interface. Since the hydrothermal grown TiO_2 not only increased the specific surface area of the nanostructured material, but also passivated the surface defects of SnO_2 photoanode, the surface recombination routes are blocked, leading to a dramatic increase on the charge recombination resistance of SnO_2 HS–TiO_2 NW photoanode. The values of R_{rec}, R_{ct}, and calculated electron lifetime (τ_r) corresponding to SnO_2 HS and SnO_2 HS–TiO_2 NW are also listed in Table I. The τ_r can be calculated from the expression: $\tau_r = 1/2\pi f_r$, where f_r is the characteristic frequency minimum of Bode figure [see Fig. 4(d)]. The calculated electron lifetime in SnO_2 HS–TiO_2 NW electrode is 100.5 ms, much longer than that in SnO_2 HS film with 15.9 ms, which suggests less charge recombination in SnO_2 HS–TiO_2 NW photoanodes owing to coating of TiO_2 on the surface of SnO_2 HS as well as the growth of TiO_2 NWs.

Figure 5 shows the *J–V* curves of DSC devices with photoanodes made of SnO_2 HS and SnO_2 HS–TiO_2 NW, respectively. Detailed parameters are listed in Table II. The highest power conversion efficiency of DSC based on SnO_2 HS–TiO_2 NW can reach 2.9%, while the only 0.4% was achieved in the DSC based on SnO_2 HS photoanode. On account of larger BET surface area with significantly more dye loading with good light-scatting ability, the short-circuit photocurrent density of SnO_2 HS–TiO_2 NW is much higher than that of SnO_2 HS.

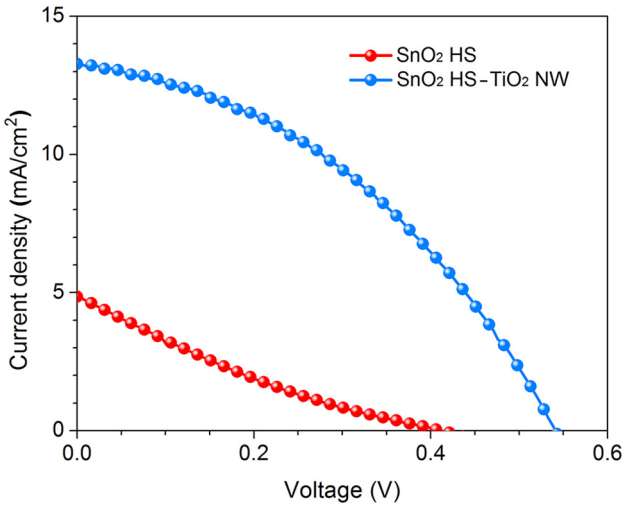

Figure 5. The *J–V* curves of the DSCs with SnO_2 HS and SnO_2 HS–TiO_2 NW photoanodes of a thickness of 20 μm and sensitized with N719.

Table II. Comparison of short-circuit current density (J_{sc}), open-circuit voltage (V_{oc}), fill factor (FF), and power conversion efficiency (η) of solar cells with SnO_2 HS and SnO_2 HS–TiO_2 NW as photoanodes, respectively.

DSCs	J_{sc} (mA/cm^2)	V_{oc} (V)	FF	η (%)
SnO_2 HS–TiO_2 NW	13.3	0.54	0.40	2.9
SnO_2 HS	4.9	0.41	0.20	0.4

https://doi.org/10.1557/mrc.2016.34 Published online by Cambridge University Press

In addition, TiO_2 NWs and coating on the surface of SnO_2 HS effectively suppress the charge recombination result in noticeable improvement on the open-circuit voltage. Since fill factor is directly related to the charge recombination resistance and charge transfer resistance (R_{rec}/R_{ct}), the surface modification with TiO_2 coating or NWs appreciably enhanced the charge recombination resistance and consequently increased the fill factor.

Conclusions

TiO_2 NW-modified SnO_2 HSs was prepared using a sequential template-free hydrothermal method for the first time, while pure and high crystallinity product were obtained. During the hydrothermal reaction process, the specific area of the photoanode was significantly increased by the formation of TiO_2 NWs, while the surface defects of SnO_2 was dramatically reduced by the interfacial passivation effect. Therefore, the dye loading and light harvesting of the composite photoanode were enhanced, while the charge recombination was successfully suppressed. Consequently, the power conversion efficiency of the solar cell based on such TiO_2 NW-modified SnO_2 HS photoanode reached 2.9%, which represented six time enhancement as compared with the DSCs with SnO_2 HS electrodes.

Acknowledgments

This work was supported by the "thousands talents" program for pioneer researcher and his innovation team, China. This work was also supported by the National Science Foundation of China (grant numbers 51374029 and 91433102), Program for New Century Excellent Talents in the University (grant number NCET-13-0668), Fundamental Research Funds for the Central Universities (grant number FRF-TP-14-008C1), and China Postdoctoral Science Foundation (grant number 2014M550675).

References

1. B. Oregan and M. Gratzel: A low-cost, high-efficiency solar-cell based on dye-sensitized colloidal TiO_2 films. *Nature* **353**, 737 (1991).
2. Y. Bai, Y.M. Cao, J. Zhang, M. Wang, R.Z. Li, P. Wang, S.M. Zakeeruddin, and M. Gratzel: High-performance dye-sensitized solar cells based on solvent-free electrolytes produced from eutectic melts. *Nat. Mater.* **7**, 626 (2008).
3. P. Wang, S.M. Zakeeruddin, J.E. Moser, M.K. Nazeeruddin, T. Sekiguchi, and M. Gratzel: A stable quasi-solid-state dye-sensitized solar cell with an amphiphilic ruthenium sensitizer and polymer gel electrolyte. *Nat. Mater.* **2**, 402 (2003).
4. K. Kakiage, Y. Aoyama, T. Yano, K. Oya, J. Fujisawab, and M. Hanaya: Highly-efficient dye-sensitized solar cells with collaborative sensitization by silyl-anchor and carboxy-anchor dyes. *Chem. Commun.* **51**, 15894 (2015).
5. E. Hendry, M. Koeberg, B. O'Regan, and M. Bonn: Local field effects on electron transport in nanostructured TiO_2 revealed by terahertz spectroscopy. *Nano Lett.* **6**, 755 (2006).
6. K. Zhu, N.R. Neale, A. Miedaner, and A.J. Frank: Enhanced charge-collection efficiencies and light scattering in dye-sensitized solar cells using oriented TiO_2 nanotubes arrays. *Nano Lett.* **7**, 69 (2007).
7. D.H. Chen, F.Z. Huang, Y.B. Cheng, and R.A. Caruso: Mesoporous anatase TiO_2 beads with high surface areas and controllable pore sizes: a superior candidate for high-performance dye-sensitized solar cells. *Adv. Mater.* **21**, 2206 (2009).
8. F. Sauvage, D.H. Chen, P. Comte, F.Z. Huang, L.P. Heiniger, Y.B. Cheng, R.A. Caruso, and M. Graetzel: Dye-sensitized solar cells employing a single film of mesoporous TiO_2 beads achieve power conversion efficiencies over 10%. *ACS Nano* **4**, 4420 (2010).
9. K.C. Huang, Y.C. Wang, R.X. Dong, W.C. Tsai, K.W. Tsai, C.C. Wang, Y. H. Chen, R. Vittal, J.J. Lin, and K.C. Ho: A high performance dye-sensitized solar cell with a novel nanocomposite film of PtNP/MWCNT on the counter electrode. *J. Mater. Chem.* **20**, 4067 (2010).
10. J. Tian and G. Cao: Control of nanostructures and interfaces of metal oxide semiconductors for quantum-dots-sensitized Solar cells. *J. Phys. Chem. Lett.* **6**, 1859 (2015).
11. Q.F. Zhang, C.S. Dandeneau, X.Y. Zhou, and G.Z. Cao: ZnO nanostructures for dye-sensitized solar cells. *Adv. Mater.* **21**, 4087 (2009).
12. Q.F. Zhang and G.Z. Cao: Nanostructured photoelectrodes for dye-sensitized solar cells. *Nano Today* **6**, 91 (2011).
13. C. Fei, J. Tian, Y. Wang, X. Liu, L. Lv, Z. Zhao, and G. Cao: Improved charge generation and collection in dye-sensitized solar cells with modified photoanode surface. *Nano Energy* **10**, 353 (2014).
14. Y. Wang, J. Tian, C. Fei, L. Lv, X. Liu, Z. Zhao, and G. Cao: Microwave-assisted synthesis of SnO_2 nanosheets photoanodes for dye-sensitized solar cells. *J. Phys. Chem. C* **118**, 25931 (2014).
15. A.N.M. Green, E. Palomares, S.A. Haque, J.M. Kroon, and J.R. Durrant: Charge transport versus recombination in dye-sensitized solar cells employing nanocrystalline TiO_2 and SnO_2 films. *J. Phys. Chem. B* **109**, 12525 (2005).
16. X.X. Xu, J. Zhuang, and X. Wang: SnO_2 quantum dots and quantum wires: controllable synthesis, self-assembled 2D architectures, and gas-sensing properties. *J. Am. Chem. Soc.* **130**, 12527 (2008).
17. D.F. Zhang, L.D. Sun, J.L. Yin, and C.H. Yan: Low-temperature fabrication of highly crystalline SnO_2 nanorods. *Adv. Mater.* **15**, 1022 (2003).
18. Z.W. Pan, Z.R. Dai, and Z.L. Wang: Nanobelts of semiconducting oxides. *Science* **291**, 1947 (2001).
19. J. Zhang, S. Li, P. Yang, W. Que, and W. Liu: Deposition of transparent TiO_2 nanotubes-films via electrophoretic technique for photovoltaic applications. *Sci. China Mater.* **58**, 785 (2015).
20. Y.L. Wang, X.C. Jiang, and Y.N. Xia: A solution-phase, precursor route to polycrystalline SnO_2 nanowires that can be used for gas sensing under ambient conditions. *J. Am. Chem. Soc.* **125**, 16176 (2003).
21. A. Kay and M. Gratzel: Dye-sensitized core-shell nanocrystals: improved efficiency of mesoporous tin oxide electrodes coated with a thin layer of an insulating oxide. *Chem. Mater.* **14**, 2930 (2002).
22. S. Ito, Y. Makari, T. Kitamura, Y. Wada, and S. Yanagida: Fabrication and characterization of mesoporous SnO_2/ZnO-composite electrodes for efficient dye solar cells. *J. Mater. Chem.* **14**, 385 (2004).
23. N.G. Park, M.G. Kang, K.M. Kim, K.S. Ryu, S.H. Chang, D.K. Kim, J. van de Lagemaat, K.D. Benkstein, and A.J. Frank: Morphological and photoelectrochemical characterization of core-shell nanoparticle films for dye-sensitized solar cells: Zn-O type shell on SnO_2 and TiO_2 cores. *Langmuir* **20**, 4246 (2004).
24. H.B. Wu, J.S. Chen, X.W. Lou, and H.H. Hng: Synthesis of SnO_2 hierarchical structures assembled from nanosheets and their lithium storage properties. *J. Phys. Chem. C* **115**, 24605 (2011).
25. M. Law, L.E. Greene, J.C. Johnson, R. Saykally, and P.D. Yang: Nanowire dye-sensitized solar cells. *Nat. Mater.* **4**, 455 (2005).
26. Y. Ohsaki, N. Masaki, T. Kitamura, Y. Wada, T. Okamoto, T. Sekino, K. Niihara, and S. Yanagida: Dye-sensitized TiO_2 nanotube solar cells: fabrication and electronic characterization. *Phys. Chem. Chem. Phys.* **7**, 4157 (2005).
27. B. Tan and Y.Y. Wu: Dye-sensitized solar cells based on anatase TiO_2 nanoparticle/nanowire composites. *J. Phys. Chem. B* **110**, 15932 (2006).
28. J.T. Jiu, S. Isoda, F.M. Wang, and M. Adachi: Dye-sensitized solar cells based on a single-crystalline TiO_2 nanorod film. *J. Phys. Chem. B* **110**, 2087 (2006).
29. L. Zhao, J.G. Yu, J.J. Fan, P.C. Zhai, and S.M. Wang: Dye-sensitized solar cells based on ordered titanate nanotube films fabricated by electrophoretic deposition method. *Electrochem. Commun.* **11**, 2052 (2009).

https://doi.org/10.1557/mrc.2016.34 Published online by Cambridge University Press

30. X.T. Yin, W.X. Que, D. Fei, H.X. Xie, and Z.L. He: Effect of TiO_2 shell layer prepared by wet-chemical method on the photovoltaic performance of ZnO nanowires arrays-based quantum dot sensitized solar cells. *Electrochim. Acta* **99**, 204 (2013).
31. H. Wang, B. Li, J. Gao, M. Tang, H.B. Feng, J.H. Li, and L. Guo: SnO_2 hollow nanospheres enclosed by single crystalline nanoparticles for highly efficient dye-sensitized solar cells. *CrystEngComm* **14**, 5177 (2012).
32. W.Q. Wu, Y.F. Xu, H.S. Rao, H.L. Feng, C.Y. Su, and D.B. Kuang: Constructing 3D branched nanowire coated macroporous metal oxide electrodes with homogeneous or heterogeneous compositions for efficient solar cells. *Angew. Chem. Int. Ed. Engl.* **53**, 4816 (2014).
33. W.Q. Wu, B.X. Lei, H.S. Rao, Y.F. Xu, Y.F. Wang, C.Y. Su, and D.B. Kuang: Hydrothermal fabrication of hierarchically anatase TiO_2 nanowire arrays on FTO glass for dye-sensitized solar cells. *Sci. Rep.* **3** (2013).
34. P. Patnaik: *Handbook of Inorganic Chemicals* (McGraw-Hill, New York, 2003).
35. S.H. Ahn, D.J. Kim, W.S. Chi, and J.H. Kim: Hierarchical double-shell nanostructures of TiO_2 nanosheets on SnO_2 hollow spheres for high-efficiency, solid-state, dye-sensitized solar cells. *Adv. Funct. Mater.* **24**, 5037 (2014).

https://doi.org/10.1557/mrc.2016.34 Published online by Cambridge University Press